Switching nonlinear optical properties by proton transfer in hydrogen-bonded merocyanine dyes: a theoretical investigation at the semi-empirical level

Pascal G. Lacroix,* Christine Lepetit and Jean Claude Daran

Laboratoire de Chimie de Coordination, CNRS, 205 route de Narbonne, 31077 Toulouse cedex, France

Received (in Montpellier, France) 20th September 2000, Accepted 17th November 2000
First published as an Advance Article on the web 21st February 2001

The synthesis of $[H(M^2)_2]^+I^- \cdot 3/2H_2O$ [M^2 being a zwitterionic cyanine dye of formula $HOCH_2CH_2$-$(NC_5H_4)CHCH(C_6H_4)O$] is reported. The crystal structure indicates that two M^2 entities share one proton in the solid state. INDO calculations reveal that the protonation strongly affects the molecular hyperpolarizability β of these dyes, while PM3 calculations indicate a potential barrier of 0.76 eV for the proton transfer between $(HM^2)^+$ and M^2. The possibility of an NLO switch for this type of compound is discussed.

Intense research activity has been devoted to nonlinear optical (NLO) materials in relation to their potential applications in telecommunications, optical computing and optical data storage.[1] The large quadratic NLO responses of donor–acceptor conjugated organic molecules is especially appealing and it is now widely believed that they have the capability to become the materials of choice for the next generations of devices.[2–5] Incorporating switchability into the NLO behavior would further increase their potential applications in emerging optoelectronic and photonic technologies. The concept of molecular switches is currently attracting great interest from various perspectives[6,7] and molecular materials with switchable quadratic NLO response have recently been reviewed.[8] Most investigations have envisaged β modulation upon molecular isomerization, in solution or polymeric matrix. Intramolecular proton transfer (tautomeric equilibrium) in salicylidene derivatives has also been reported in the crystalline state.[9]

Along this line, we wish to report here on a theoretical investigation of the effect of intermolecular proton transfer on the NLO response of a pair of chromophores. In order to provide a benchmark structure for this investigation, we have tried to embody two-proton acceptor chromophores in a hydrogen-bonded network offering proton vacancies to favor intermolecular proton interactions. For these investigations, the zwitterionic merocyanine dye M^2 (Scheme 1) has been selected. M^2 derives from a well-known chromophore (M^1, Scheme 1), which has been widely investigated for its exceptionally large molecular hyperpolarizability ($\beta \approx 1000 \times 10^{-30}$ cm^5 esu^{-1}).[10–13] In a previous investigation, the hyperpolarizability of M^2 was found to be similar to that of the well known M^1 dye, in relation to identical "push-pull" π-electronic structures for both dyes.[14] Besides a large β value, the reason for selecting this family was related to the fact that the protonation of the phenolate would strongly reduce the donor strength of the substituent and hence the hyperpolarizability, providing a simple strategy for NLO switching upon proton transfer. M^2 was preferred instead of M^1 for its long range hydrogen-bonding capabilities, which could favor long-range proton interactions and promote acentric alignments of chromophores, following a strategy which has been successful in previous structural studies involving this dye.[14,15]

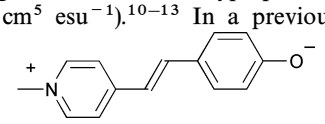

M^1

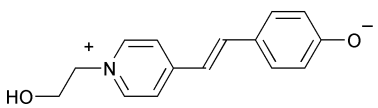

M^2

Scheme 1

In the first section we report the synthesis and crystal structure of $[H(M^2)_2]^+I^- \cdot 3/2H_2O$, a salt in which two M^2 chromophores share one proton located on one entity, but strongly involved in a hydrogen-bonded network. The crystal is centrosymmetric and, therefore, has no macroscopic NLO response. However, spectroscopy and INDO calculations provide evidence for a large β modulation of M^2 upon protonation. In the last section, a theoretical investigation of the effect of proton transfer within the $[H(M^2)_2]^+$ unit is presented in relation to the concept of NLO switchability.

Experimental

Materials and equipment

Starting materials were used as purchased without further purification. M^2 was synthesized as previously reported.[14] UV/Vis spectra were recorded on a Hewlett Packard 8452A spectrophotometer and ^{1}H NMR spectra on a Bruker AM 250 spectrometer. As M^2 is extremely sensitive to traces of acid, it was essential to maintain the basicity of the solvent by addition of a small amount of amine, according to the procedure already reported,[16,17] for recording the spectra of pure M^2. Elemental analyses were performed by the Service de Microanalyses du CNRS in the Laboratoire de Chimie de Coordination (Toulouse). Thermal measurements were performed by TG/DTA (thermogravimetric/differential thermoanalysis) on a Setaram TGDTA92 thermoanalyser.

Synthesis of $[H(M^2)_2]^+I^- \cdot 3/2H_2O$

The following procedure is a modification of that previously described for M^2.[14] 2-Iodoethanol (3.44 g, 2×10^{-2} mol) was

mixed with 10 ml (large excess) of 4-picoline and stirred overnight at room temperature. The excess of picoline was carefully removed under vacuum. To the residual yellow oil were successively added 50 ml of 2-propanol, 2.44 g (2×10^{-2} mol) of 4-hydroxybenzaldehyde and 1 ml of piperidine. The resulting red mixture was refluxed for 24 h. After cooling, a large amount of reddish solid was filtered off, washed with 2-propanol and dried under vacuum (78% yield). ^{1}H NMR (DMSO-d_6): δ 3.925 (t, $J = 4.6$, 2H), 4.53 (t, $J = 4.6$, 2H), 6.73 (m, 2H), 7.14 (d, $J = 15.1$, 1H), 7.62 (d, $J = 8.1$, 2H), 7.97 (d, $J = 15.7$ Hz, 1H), 8.07 (m, 2H), 8.70 (m, 2H). TG analysis indicates a loss of 1.075% at 50–100 °C, which is consistent with 0.34 residual water per $[H(M^2)_2]^+$ entity in the sample. Anal. calc. (found) for $C_{30}H_{31}IN_2O_4 \cdot 1/3H_2O$: C, 58.45 (58.60); H, 5.18 (4.86); N, 4.55 (4.56%). Recrystallization from boiling water affords orange–red crystals of formula $[H(M^2)_2]^+I^- \cdot 3/2H_2O$ (72% yield).

X-Ray structure determination

The data were collected on a Stoe imaging plate diffraction system (IPDS). The final unit cell parameters were obtained by the least-squares refinement of 5000 reflections. Only statistical fluctuations were observed in the intensity monitors over the course of the data collection. An empirical absorption correction was applied.

The structure was solved by direct methods (SIR92)[18] and refined by least-squares procedures on F_{obs}. H atoms were located on difference Fourier maps, but those attached to C atoms were introduced in idealized positions [d(CH) = 0.96 Å] and their atomic coordinates were recalculated after each cycle. They were given isotropic thermal parameters 20% higher than those of the carbon to which they are attached. The coordinates of the H atoms attached to the O atoms were refined but the O–H distances and C–O–H or O–H···O angles were restrained to their mean values. They were given an equivalent isotropic thermal parameter. Least-squares refinements were carried out by minimizing the function $\Sigma w(|F_o| - |F_c|)^2$, where F_o and F_c are the observed and calculated structure factors. The weighting scheme used in the last refinement cycles was $w = w'[1 - (\Delta F/6\sigma(F_o)^2]^2$, where $w' = 1/\Sigma_1^n A_r T_r(x)$ with 3 A_r coefficients for the Chebyshev polynomial $A_r T_r(x)$ where x is F_c/F_c(max).[19] Models reached convergence with $R = \Sigma(||F_o| - |F_c||)/\Sigma(|F_o|)$ and $wR = [\Sigma w(|F_o| - |F_c|)^2/\Sigma w(F_o)^2]^{1/2}$ having the values listed in Table 1. Details of data collection and refinement are given in Table 1.

The calculations were carried out with the CRYSTALS package of programs.[20] The drawing of the molecule was realized with CAMERON.[21]

CCDC reference number 440/242. See http://www.rsc.org/suppdata/nj/b0/b007726g/ for crystallographic files in .cif format.

Table 1 Crystal data for $[H(M^2)_2]^+I^- \cdot 3/2H_2O$

Formula	$[(C_{15}H_{16}NO_2)_2(C_{15}H_{15}NO_2)_2 \cdot 3H_2O]\ I_2$
FW	1275.03
Crystal system	Triclinic
Space group	$P\bar{1}$
a/Å	8.8875(9)
b/Å	11.9248(12)
c/Å	26.990(3)
α/°	91.41(1)
β/°	94.48(1)
γ/°	99.52(1)
U/Å^3	2810.4(5)
Z	2
T/K	180
μ(Mo-Kα)/cm^{-1}	11.671
Reflections collected	17 533
Unique reflections (R_{int})	8306 (0.0352)
Reflections used ($I > 2\sigma(I)$)]	6529
R	0.0283
wR	0.0330

Computational details

The all-valence INDO (intermediate neglect of differential overlap) method,[22] in connection with the sum-over-state (SOS) formalism,[23] was employed for the calculation of the molecular hyperpolarizability β (-2ω; ω, ω) of M^2 and $(HM^2)^+$. Structural parameters used for the INDO calculations were taken from the present crystal study. Details of the computationally efficient INDO-SOS-based method for describing second-order molecular optical nonlinearities have been reported elsewhere.[24] Calculations were performed using the INDO/1 Hamiltonian incorporated in the commercially available MSI software package ZINDO.[25] The monoexcited configuration interaction (MECI) approximation was employed to describe the excited states. The 100 energy transitions between the ten highest occupied molecular orbitals and the ten lowest unoccupied ones were chosen to undergo CI mixing.

A partially relaxed potential energy surface was evaluated for the proton transfer within a $[H(M^2)_2]^+$ unit, at the semi-empirical level using PM3 included in GAUSSIAN94.[26] The system made of molecules **1** and **2** (see Description of the structure) was selected for the calculation. The O–H distance was varied from 0.930 to 1.270 Å in 0.03 Å steps and moving the proton from $(HM^2)^+$ toward M^2. For each fixed O–H distance, a partial geometry optimization of a model containing two chromophores and the water molecules in hydrogen-bonding interaction with them was performed. The phenolic oxygen, and those of the water molecules, were maintained fixed whereas the proton and the hydrogen atoms of the water molecules were allowed to move freely. In order to consistently model a proton transfer in the solid state, the relative chromophore orientation was fixed and only the intramolecular distances were allowed to relax. A vibrational analysis was performed upon geometry optimization for the models with O–H bond lengths of 0.960 and 1.236 Å. In the latter, a large imaginary frequency located at 2656 cm^{-1} associated with the elongation of the phenol O–H bond is obtained, suggesting that the corresponding structure is a transition state in the proton transfer from $(HM^2)^+$ to M^2. Weak imaginary frequencies are also obtained at low wavenumbers in both cases and are associated with rotations, translations or chromophore deformations expected to be forbidden in the solid state.

Results and discussion

Description of the structure of $[H(M^2)_2]^+I^- \cdot 3/2H_2O$

The asymmetric unit is shown in Fig. 1, while selected bond lengths are collected in Table 2. The structure is built up from four independent molecules (labeled **1**–**4** according to Fig. 1), three water molecules and two iodide ions which are linked through a hydrogen-bond network. Of the four molecules, two

Table 2 Interatomic distances (Å) for $[H(M^2)_2]^+I^- \cdot 3/2H_2O$. ESDs in parentheses refer to the last significant digit

Molecule **1** (phenol)		Molecule **4** (phenol)	
O11–C11	1.351(3)	O41–C41	1.352(3)
O11–H11	0.88(2)	O41–H41	0.86(12)
C14–C141	1.456(4)	C44–C441	1.458(4)
C141–C142	1.341(4)	C441–C442	1.342(4)
C142–C143	1.459(4)	C442–C443	1.447(4)
O12–H12	0.88(2)	O42–H42	0.87(2)
Molecule **2** (phenolate)		Molecule **3** (phenolate)	
O21–C21	1.345(3)	O31–C31	1.335(3)
C24–C241	1.449(4)	C34–C341	1.448(4)
C241–C242	1.343(4)	C341–C342	1.348(4)
C242–C243	1.456(4)	C342–C343	1.451(4)
O22–H22	0.87(2)	O32–H32	0.87(2)

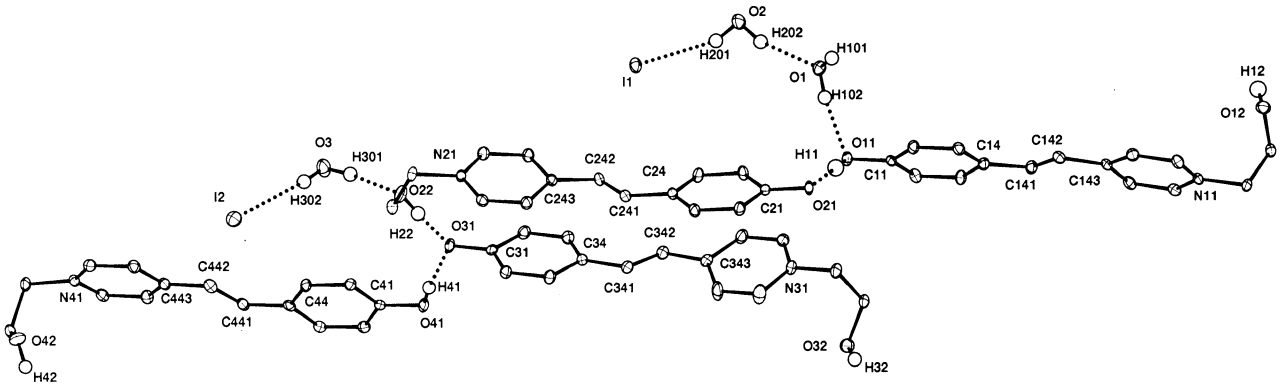

Fig. 1 Asymmetric unit cell for $[H(M^2)_2]^+I^- \cdot 3/2H_2O$, illustrating the hydrogen bonds between the four independent molecules, the water molecules and the iodide. Ellipsoids represent 30% probability level. O11, O21, O31, and O41 refer to molecules **1**, **2**, **3** and **4**, respectively.

contain a phenol group whereas the two other possess a phenolate group. Each OH group is hydrogen bonded to the O atom of one phenolate. The O atom O11 of one phenol is engaged in hydrogen bonding with water molecules O1. Each pair of phenol-phenolate molecules are connected through hydrogen bonds occurring between the oxygen O22 of the alcohol group and the O31 atom. There are also hydrogen interactions between the water molecules (H_2O2 and H_2O3) and the iodide anions. Moreover, there are intricate H bonds that connect all the molecules together, thus developing a three dimensional network. This network may be described as constituted of two different systems. The first system, shown in Fig. 2 is built up around an inversion center: each group of four molecules described above is related to its centrosymmetric counterpart through hydrogen bonds involving the water molecules H_2O1 and the phenol OH groups, as shown in Fig. 2. Moreover, the water molecule H_2O2 interacts with the H atom of an alcohol group belonging to another symmetry related molecule, whereas the oxygen O21 of the phenolate group is connected to the oxygen O42 of the alcohol group of a different symmetry-related molecule. The O–H distances in this subunit are gathered in Table 3. The second system is developed around the O31 phenolate oxygen, as shown in Fig. 3. This O31 is connected through H bonds to three O atoms, two of them, O41 and O22, belong to the initial asymmetric unit, whereas the third one, O12A, belongs to a different symmetry-related molecule.

Optical spectroscopy

The electronic spectra of M^2 recorded under various conditions are gathered in Fig. 4. It can be seen that $[H(M^2)_2]^+I^- \cdot 3/2H_2O$ exhibits two absorption maxima (λ_{max}) located at 400 and 514 nm. In contrast, the pure M^2 compound has a single intense transition ($\lambda_{max} = 510$ nm, $\varepsilon = 39\,340$ dm^3 mol^{-1} cm^{-1}), while with an excess of CF_3COOH, $(HM^2)^+$ displays a single but more intense transition located at 400 nm ($\varepsilon = 53\,730$ dm^3 mol^{-1} cm^{-1}). Therefore, the spectrum of $[H(M^2)_2]^+I^- \cdot 3/2H_2O$ can be readily ascribed to a mixture of M^2 and $(HM^2)^+$ in solution, which indicates that the protons are localized on one-half of the dye molecules. INDO calculations provide a rationale for the above trend (Table 4). The data reveal single intense transitions located at 555–560 and 400–405 nm for M^2 and $(HM^2)^+$, respectively. A blue shift upon protonation is clearly evidenced by this calculation, in agreement with the experimental spectra.

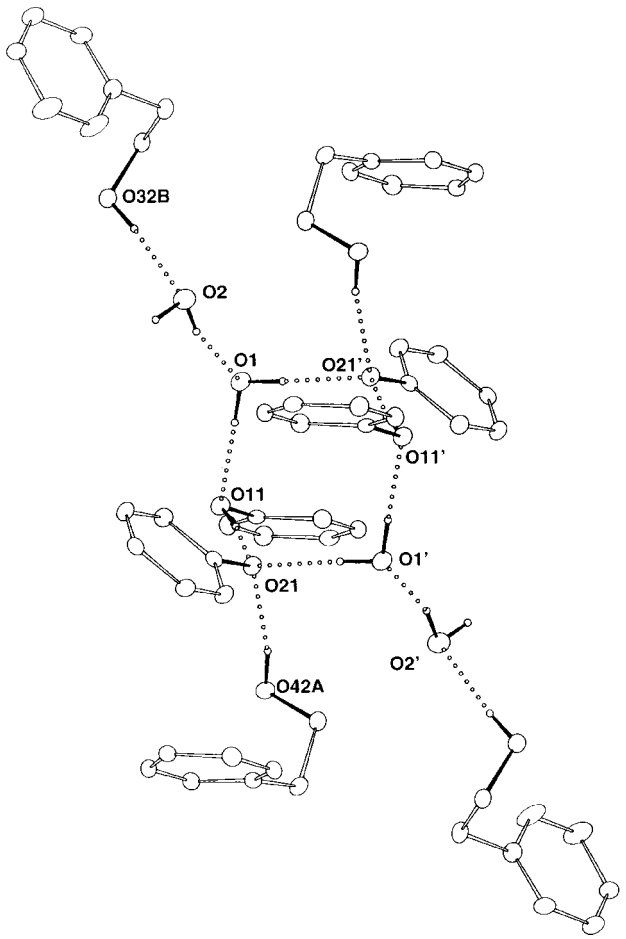

Fig. 2 Hydrogen-bonding network around the O11–H11···O21 unit. Symmetry transformations used to generate equivalent atoms: $' = -x, -y, -z$; A $= 1 - x, 1 - y, -z$; B $= x, y - 1, z$.

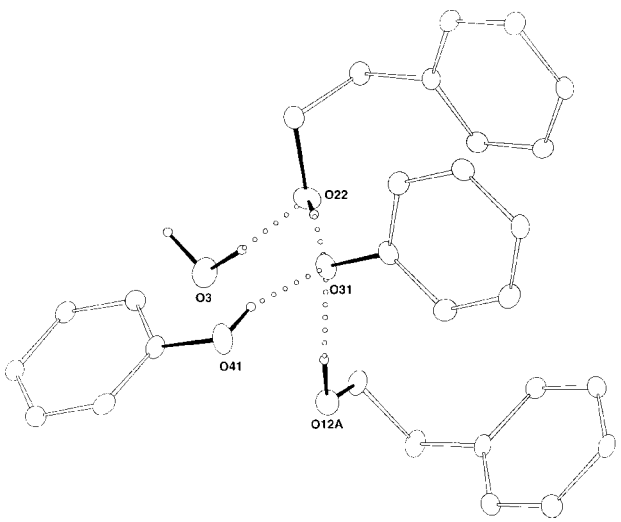

Fig. 3 Hydrogen-bonding network around the O41–H41···O31 unit. Symmetry transformation used to generate equivalent atoms: A $= 1 - x, 1 - y, -z$.

Table 3 Hydrogen bonds (D–H···A) within the O11–H11···O21 system

D–H···A	d(D–H)/Å	d(H···A)/Å	∠DHA/°	d(D···A)/Å
O11–H11···O21	0.88(2)	1.60(2)	170(3)	2.469(3)
O12–H12···O31[a]	0.88(2)	1.84(2)	174(2)	2.719(3)
O22–H22···O31	0.87(2)	1.71(2)	166.7(7)	2.564(3)
O32–H32···O2[b]	0.87(2)	1.92(2)	173(1)	2.784(3)
O41–H41···O31	0.86(2)	1.71(2)	163(3)	2.550(3)
O42–H42···O21[c]	0.87(2)	1.90(2)	167(2)	2.756(3)
O1–H101···O21[d]	0.90(2)	1.89(2)	176(3)	2.791(3)
O1–H102···O11	0.90(2)	1.97(2)	168(3)	2.854(3)
O2–H201···I1	0.90(2)	2.61(2)	158(2)	3.465(2)
O2–H202···O1	0.90(2)	1.99(2)	162(2)	2.869(3)
O3–H301···O22	0.92(2)	1.87(2)	173(3)	2.788(3)
O3–H302···I2	0.95(2)	2.56(2)	160(2)	3.470(2)

[a] $-x+1, -y+1, -z+1$. [b] $x, y+1, z$. [c] $-x+1, -y+1, -z$. [d] $-x+2, -y+1, -z+1$.

Molecular hyperpolarizabilities β

It has previously been reported that M^1 and M^2 exhibit hyperpolarizabilities related to their push-pull π-electronic structures.[10–15] Therefore, the present section will focus instead on a comparison of the β value between M^2 and $(HM^2)^+$. The theoretical values calculated for every M^2 and $(HM^2)^+$ fragment present in the unit cell are gathered in Table 5. The frequency dependence of β is clearly evidenced from the data. The values calculated at 1.064 μm are strongly enhanced by resonance in the case of M^2; they become irrelevant and, therefore, they are not reported in the table. The negative signs of β indicate a reduction of the dipole moment ($\Delta\mu < 0$) between the ground and excited states in the transitions responsible for the NLO response. Moreover, after protonation β decreased by a factor of 5 to 7 relative to M^2 depending on the frequency.

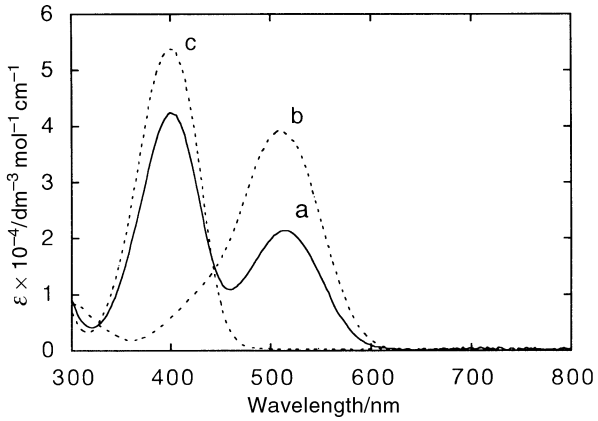

Fig. 4 Electronic spectrum of $[H(M^2)_2]^+I^-$ (a) recorded in ethanol. M^2 is shown as a reference in pure ethanol (dotted line b) and in acidic (CF_3COOH) ethanolic solution (dotted line c).

Within the framework of SOS perturbation theory β is related to all excited states and can be partitioned into two contributions (β_{2level} and β_{3level}). Analysis of the term contributions in Table 5 reveals that the two-level terms dominate the nonlinearity, with positive β_{3level} values roughly 2 to 5 times lower than the negative β_{2level} values, depending on the molecule. Therefore, we make the assumption that understanding β_{2level} will provide a satisfactory understanding of β. β_{2level} can be related to the first low-lying transitions (labeled $1 \rightarrow 2$) for both $(HM^2)^+$ and M^2 (Table 4). These transitions contribute about 90 and 98% of the nonlinearity of $(HM^2)^+$ and M^2, respectively (State $\% = \beta_{1\rightarrow 2}/\sum_{n=2}^{n=101} \beta_{1\rightarrow n}$). They essentially involve the HOMO → LUMO transitions. Both orbitals are shown in Fig. 5. The role of phenolate protonation is especially important at the HOMO level, which undergoes a large switch in energy from −6.11 to −10.52 eV, and consequently a blue shift in the $1 \rightarrow 2$ transition energy (ΔE). This modification appears to be the dominant parameter accounting for the 5 to 7 times reduction in β observed on going from M^2 to $(HM^2)^+$ (see Table 5), according to the

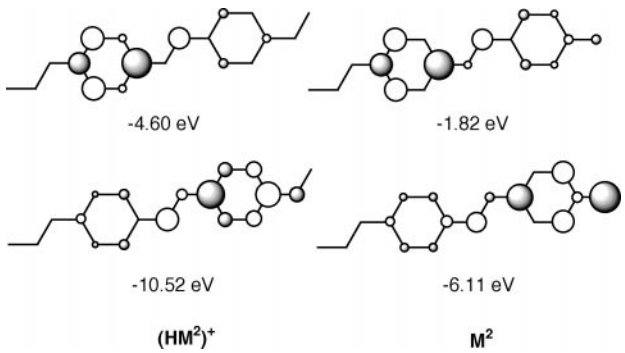

Fig. 5 Frontier orbital HOMO (bottom) and LUMO (top) for $(HM^2)^+$ and M^2.

Table 4 INDO calculated energies (λ_{max}), oscillator strengths (f), dipole moment changes between ground and excited state ($\Delta\mu$), and composition of the first excited state for M^2 and $(HM^2)^+$

Compound	Transition[a]	λ_{max}/nm	f	$\Delta\mu$/D	Composition of CI expansion[b]
$(HM^2)^+$					
Molecule **1**	$1 \rightarrow 2$	400	1.1	− 14.7	0.954 χ46 → 47
Molecule **4**	$1 \rightarrow 2$	405	1.1	− 14.5	0.954 χ46 → 47
M^2					
Molecule **2**	$1 \rightarrow 2$	557	1.9	− 13.2	0.965 χ46 → 47
Molecule **3**	$1 \rightarrow 2$	559	1.9	− 13.4	0.966 χ46 → 47

[a] 1 is the ground state and 2 is the first excited state. [b] Expansion of the electronic transition over the excited state orbitals in the configuration interaction (CI) formalism. In both cases, there is only one component with a large coefficient. Orbital 46 is the HOMO and 47 is the LUMO in all cases.

Table 5 Molecular hyperpolarizabilities ($\beta_{total} = \beta_{2level} + \beta_{3level}$) calculated at different laser frequencies for M^2 and $(HM^2)^+$, on the basis of the crystal data. The negative signs indicate a reduction of the dipole moment ($\Delta\mu < 0$) in the electronic transitions

	Hyperpolarizability/10^{-30} cm^5 esu^{-1}							
	$(HM^2)^+$				M^{2+}			
	Molecule **1**		Molecule **4**		Molecule **2**		Molecule **3**	
Wavelength/ μm	β_{total}	β_{2level}	β_{total}	β_{2level}	β_{total}	β_{2level}	β_{total}	β_{2level}
∞	−49.7	−93.2	−52.7	−96.8	−276	−361	−274	−361
1.907	−66.0	−115	−70.6	−121	−476	−592	−475	−595
1.064	−158	−234	−175	−254	Resonance		Resonance	

widely-used two-level description of the quadratic NLO response:[27]

$$\beta_{zzz} = \frac{3e\hbar^2 f\Delta\mu}{2m(\Delta E)^3} \times \frac{(\Delta E)^4}{[(\Delta E)^2 - (2\hbar\omega)^2][(\Delta E)^2 - (\hbar\omega)^2]}$$

In this relation, β_{zzz} is the tensor component along the charge transfer axis (OZ) of the molecule, $\hbar\omega$ is the energy of the laser beam, and f is the oscillator strength of the transition. A large β dependence upon proton delocalization could offer a potentially useful mechanism for NLO switching within a $[H(M^2)_2]^+$ entity. This possibility will be envisioned in the next section.

A possibility for switching the hyperpolarizability by proton delocalization.

Experimental evidence for proton transfer in $[H(M^2)_2]^+I^- \cdot 3/2H_2O$ can be obtained by NMR spectroscopy. The ^{1}H NMR data recorded under various conditions are gathered in Table 6. The spectrum of pure $[H(M^2)_2]^+I^- \cdot 3/2H_2O$ appears to be a mixture of those of M^2 and $(HM^2)^+$, which indicates a localization of less than 10^{-6} s for the proton on each M^2 chromophore. More interestingly, having a crystal made of mixed protonated/deprotonated entities strongly interacting raises the question of possible transfer in the solid state, which would be most interesting for further application in materials science.

The entity composed of molecules **1** and **2** (see Table 2) offers the best perspectives for this investigation with a short O–O distance [O11–O21 = 2.469(3) Å], which implies a strong hydrogen bond. The model used in the PM3 geometry optimizations is made of molecules **1** and **2** with three hydrogen-bonded water molecules (Fig. 6). For simplicity, a water molecule was used instead of the O42-based hydroxyethyl fragment. The calculated geometry modifications occurring in the M^2 dyes upon proton motion are illustrated in Table 7, for selected bond lengths. It can be easily seen that the two entities become identical in the transition state, when the O11–H11 distance is equal to the half of the O11–O21 separation. The variation of the total energy of the $[H(M^2)_2]^+$ entity with the O11–H11 distance is shown in Fig. 7. The lowest energy is found for a O–H bond length equal to 0.96 Å, in striking contrast to the 0.88 Å observed by X-ray diffraction. However, it is well known that determining the precise position of hydrogens from X-ray crystallographic data is not possible. It is commonly assumed that the true bond length is about 0.12 Å longer than the value measured by X-ray diffraction, which makes the O11–H11 distance probably around 1 Å. Taking this into account makes the agreement between calculation and experiment more satisfactory. More importantly, the figure indicates a potential barrier equal to 0.76 eV for the transfer process. This value, compared to the energy of a standard O–H bond (4.8 eV),[28] is indicative of proton transfer capabilities, but is higher than that usually observed for this range of O–O distances.[29] The bending of the hydrogen bond can partially account for this effect,[30] as well as the presence of solvent molecules. It is also known that electron correlation is necessary to obtain a precise value for the proton transfer energy barrier.[31] Although the present calculation has been

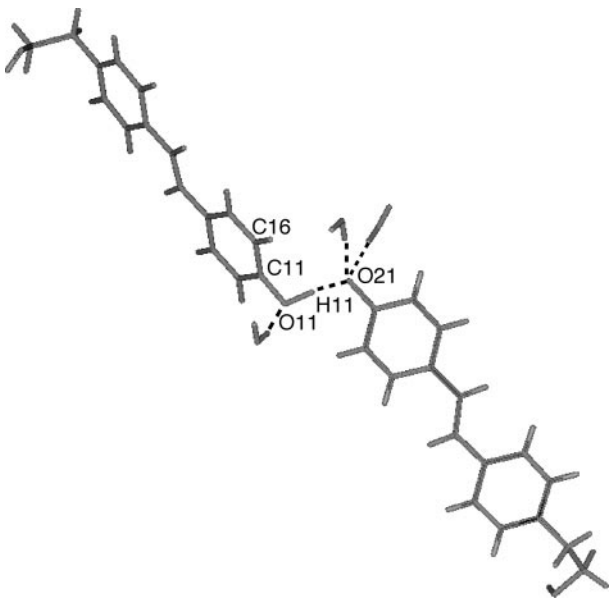

Fig. 6 Model used for PM3 geometry optimization.

Table 6 Selected ^{1}H NMR data[a] for $[H(M^2)_2]^+I^- \cdot 3/2H_2O$ (middle) compared to those of M^2 (left) and $(HM^2)^+CF_3COO^-$ (right) in DMSO-d_6.

M^2	$[H(M^2)_2]^+I^- \cdot 3/2H_2O$	$(HM^2)^+$
3.87 (t, 4.9 Hz, 2H)	3.92 (t, 4.6 Hz, 4H)	3.95 (t, 4.8 Hz, 2H)
4.34 (t, 4.6 Hz, 2H)	4.53 (t, 4.6 Hz, 4H)	4.63 (t, 4.7 Hz, 2H)
6.25 (d, 8.6 Hz, 2H)	6.73 (d, 7.0 Hz, 4H)	6.99 (d, 8.5 Hz, 2H)
6.66 (d, 15.8 Hz, 1H)	7.14 (d, 15.1 Hz, 2H)	7.40 (d, 16.3 Hz, 1H)
7.43 (d, 8.8 Hz, 2H)	7.62 (d, 8.1 Hz, 4H)	7.73 (d, 8.6 Hz, 2H)
7.67 (d, 6.4 Hz, 2H)	8.07 (s, 4H)	8.26 (d, 6.8 Hz, 2H)
7.81 (d, 15.2, 1H)	7.97 (d, 15.7 Hz, 2H)	8.01 (d, 16.3 Hz, 1H)
8.30 (d, 6.5 Hz, 2H)	8.70 (s, 4H)	8.90 (d, 6.7 Hz, 2H)

[a] Chemical shift (multiplicity, coupling constant, intensity).

Table 7 Selected bond lengths (Å) in M^2 for various O–H separations, calculated by PM3. The transition state is underlined.

	Molecule **1** (phenol)		Molecule **2** (phenolate)	
O11–H11	C11–O11	C141–C142	C21–O21	C241–C242
0.93	1.349	1.363	1.258	1.401
0.96	1.347	1.363	1.259	1.401
0.99	1.346	1.363	1.261	1.400
1.02	1.344	1.363	1.261	1.399
1.050	1.342	1.364	1.262	1.399
1.085	1.339	1.364	1.263	1.399
1.120	1.335	1.365	1.264	1.399
1.15	1.333	1.366	1.266	1.398
1.174	1.317	1.373	1.290	1.385
1.205	1.31	1.376	1.297	1.382
1.236	1.304	1.379	1.303	1.379
1.27	1.297	1.382	1.309	1.375

performed at the semi-empirical level, which is calibrated against experiment, this approach lacks a precise electron correlation treatment. Therefore, the potential barrier expected from higher level calculations, such as post Hartree–Fock or density functional theory (DFT) methods would probably be reduced. Unfortunately, these methods are not applicable to large size systems, such as $[H(M^2)_2]^+$.

The structural and NLO features encountered in $[H(M^2)_2]^+I^- \cdot 3/2H_2O$ suggest a strategy for a model of interplay between intermolecular charge delocalization and NLO response at the molecular level. In the present material, $[M^2\text{–}H\cdots M^2]^+$ and $[M^2\cdots H\text{–}M^2]^+$ give rise to NLO responses having roughly the same magnitude, but in different directions. The idealized NLO switch in such a device is illustrated in Scheme 2. In the upper part of the scheme, the resulting β is directed along OX. A laser beam propagating along OY and polarized along OX would provide the largest possible NLO response. In contrast, the situation depicted in the lower part of the scheme, which arises from proton transfer, gives a β directed along OY, and therefore a strictly vanishing NLO response. More generally, the switch in β direction (θ) has been calculated in Fig. 8 for various $\beta(M^2)/\beta(HM^2)^+$ ratios and various angles (α) between the M^2 and $(HM^2)^+$ chromophores. In the present material, α lies around 178° and the $\beta(M^2)/\beta(HM^2)^+$ ratio is equal to 7. These values indicate a θ value close to 176°, far from the 90° required for an idealized switch. In order to get more suitable combinations of parameters, two possible strategies are evidenced from the figure: lowering α by means of bulky or chiral groups

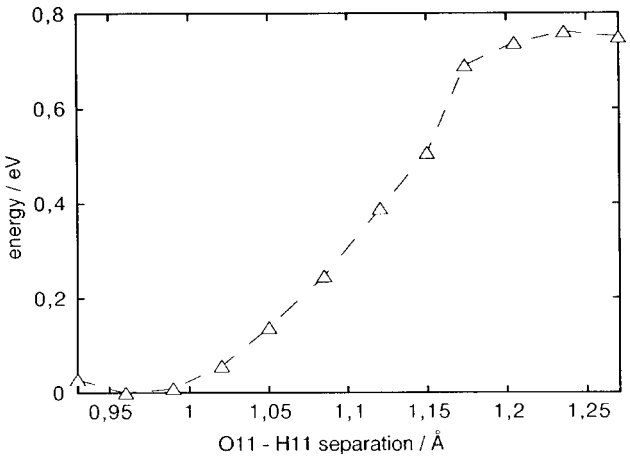

Fig. 7 PM3 energy of the $[M^2 - H\cdots M^2]^+$ entity calculated for various O–H bond lengths.

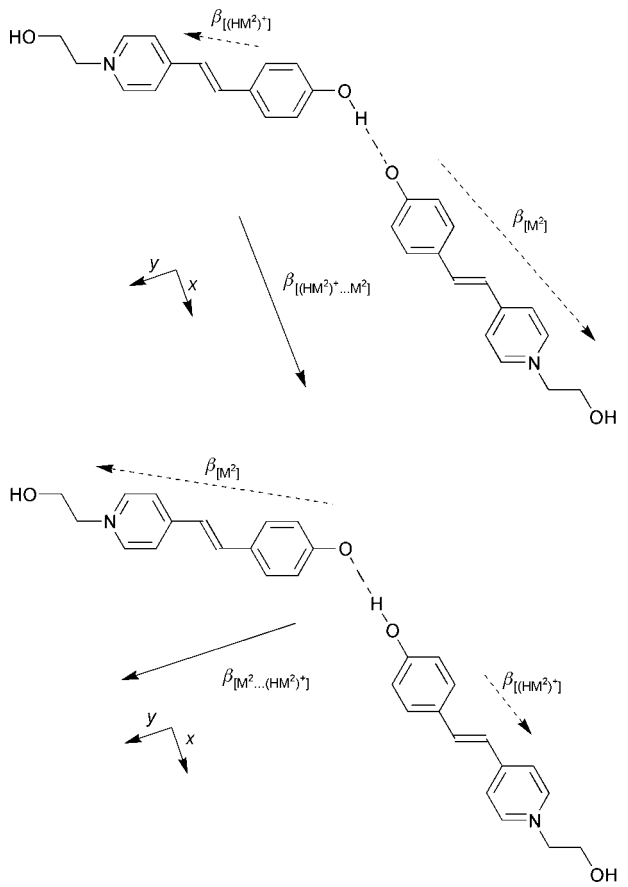

Scheme 2

on the M^2 skeleton, or lowering $\beta(M^2)/\beta(HM^2)^+$, for example by increasing the strength of the hydrogen bonding.

From the perspective of materials applications, the question of the achievement of an actual proton transfer is naturally addressed in these structures. Protonic conductors are well known transparent structures fully suitable for NLO applications.[29,32–34] They exhibit typical static potential barriers around 0.5 eV,[35] which indicates that the situation encountered within a $[H(M^2)_2]^+$ entity is compatible for solid state proton delocalization. On the other hand, the present O···H bonded network is localized on a limited number of sites (up to 12 oxygen atoms around the O11–O21 subunit), and not on the entire crystal. Consequently, there is no hope for long range proton delocalization and, therefore,

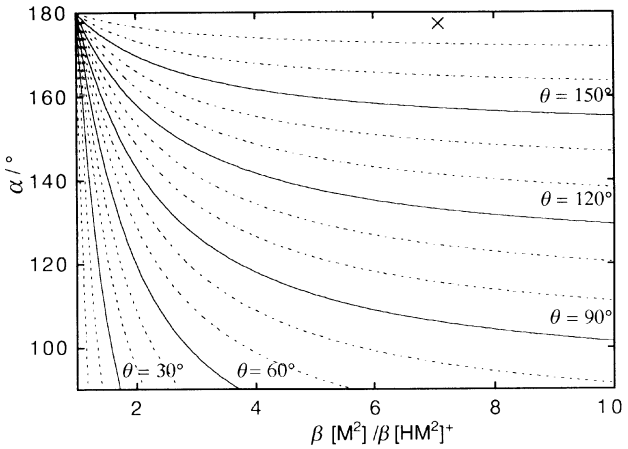

Fig. 8 Switch angle θ in the hyperpolarizability of a $[H(M^2)_2]^+$ pair after proton transfer, calculated as a function of the angle α between the two M^2 chromophores, and the ratio $\beta(M^2)/\beta(HM^2)^+$. The idealized switch depicted in Scheme 2 corresponds to $\theta = 90°$. (× indicates the situation encountered from the actual crystal structure.)

$[H(M^2)_2]^+I^- \cdot 3/2H_2O$ cannot be a protonic conductor. Further attemps to extend the hydrogen bonding network could benefit from the use of alternative counter anions capable of extended hydrogen interactions. Experiments with PO_4^{3-}, HPO_4^{2-} and $H_2PO_4^-$ are currently in progress.

Conclusions

Molecular materials solid state engineering is highly laborious, with many attempts frequently being uncertain. However, theoretical calculations based on chemical models might profoundly stimulate the science of materials design. Up to now, the intermolecular proton transfer–NLO properties relationship has received very little attention,[36] and the applications for possible NLO switches have not been envisaged. In the present communication, the possibility of interplay between both properties has been investigated on the $[H(M^2)_2]^+I^- \cdot 3/2H_2O$ model compound. This new system embodies two M^2 dyes linked together by a proton, through a strong O–H···O interaction. The main features of the hydrogen bond suggest some ability for proton jumping within a $[H(M^2)_2]^+$ entity, with a short O–O separation, and a reduced potential barrier equal to 0.76 eV. The hyperpolarizability of $(HM^2)^+$ is found to be 7 times less than that of M^2, which indicates that the charge delocalization would result in a 176° switch of the hyperpolarizability of the $[H(M^2)_2]^+$ pair. These investigations suggest that such molecular devices combining highly polarizable dyes and extended hydrogen-bonded networks could deserve more attention as building blocks for molecular materials with switchable NLO behavior.

References

1 B. E. A. Saleh and M. C. Teich, *Fundamentals of Photonics*, John Wiley, New York, 1991.
2 (*a*) *Introduction to Nonlinear Optical Effects in Molecules and Polymers*, ed. N. P. Prasad and D. J. Williams, Wiley, New York, 1991; (*b*) *Molecular Nonlinear Optics: Materials, Physics and Devices*, ed. J. Zyss, Academic Press, Boston, 1994; (*c*) *Nonlinear Optics of Organic Molecules and Polymers*, ed. H. S. Nalwa and S. Miyata, CRC Press, New York, 1997.
3 (*a*) L. R. Dalton, A. W. Harper, R. Ghosn, W. H. Steier, M. Ziari, H. Fetterman, Y. Shi, R. V. Mustacich, A. K. Y. Jen and K. J. Shea, *Chem. Mater.*, 1995, **7**, 1060; (*b*) T. Verbiest, S. Houbrechts, M. Kauranen, K. Clays and A. Persoons, *J. Mater. Chem.*, 1997, **7**, 2175.
4 *Optical Nonlinearities in Chemistry*, special issue of *Chem. Rev.*, 1994, **94**(1).
5 D. J. Williams, *Angew. Chem., Int. Ed. Engl.*, 1984, **23**, 690.
6 *Supramolecular Chemistry: Concepts and Perspectives*, ed. J. M. Lehn, VCH, Weinheim, 1995.
7 M. D. Ward, *Chem. Soc. Rev.*, 1995, **24**, 121.
8 B. J. Coe, *Chem. Eur. J.*, 1999, **5**, 2464.
9 K. Nakatani and J. Delaire, *Chem. Mater.*, 1997, **9**, 2682.
10 C. Flytzanis and A. Dulic, *Opt. Commun.*, 1978, **25**, 402.
11 B. F. Levine, C. G. Bethea, E. Wasserman and L. Leenders, *J. Chem. Phys.*, 1978, **68**, 5042.
12 G. L. Gaines, *Angew. Chem., Int. Ed. Engl.*, 1987, **26**, 341.
13 F. Pan, M. S. Wong, V. Gramlich, C. Bosshard and P. Günter, *Chem. Commun.*, 1996, 1557.
14 P. G. Lacroix, J. C. Daran and P. Cassoux, *New J. Chem.*, 1998, **22**, 1085.
15 (*a*) M. S. Wong, F. Pan, C. Bosshard and P. Günter, *Polym. Mater. Sci. Eng.*, 1996, **75**, 132; (*b*) F. Pan, M. S. Wong, V. Gramlich, C. Bosshard and P. Günther, *J. Am. Chem. Soc.*, 1996, **118**, 6315; (*c*) M. S. Wong, F. Pan, V. Gramlich, C. Bosshard and P. Günther, *Adv. Mater.*, 1997, **9**, 554.
16 (*a*) J. Catalan, P. Pérez, J. Elguero and W. Meutermans, *Chem. Ber.*, 1993, **126**, 2445; (*b*) J. Catalan, E. Mena, W. Meutermans and J. Elguero, *J. Phys. Chem.*, 1992, **96**, 3615.
17 P. Jacques, *J. Phys. Chem.*, 1986, **90**, 5535.
18 A. Altomare, G. Cascarano, G. Giacovazzo, A. Guagliardi, M. C. Burla, G. Polidori and M. Camalli, *J. Appl. Crystallogr.*, 1994, **27**, 435.
19 E. Prince, *Mathematical Techniques in Crystallography*, Springer Verlag, Berlin, 1982.
20 D. J. Watkin, C. K. Prout, J. R. Carruthers and P. W. Betteridge, CRYSTALS, Issue 11, Chemical Crystallography Laboratory, University of Oxford, Oxford, UK, 1999.
21 D. J. Watkin, C. K. Prout and L. J. Pearce, CAMERON, Chemical Crystallography Laboratory, University of Oxford, Oxford, UK, 1996.
22 M. Zerner, G. Loew, R. Kirchner and U. Mueller-Westerhoff, *J. Am. Chem. Soc.*, 1980, **102**, 589.
23 J. F. Ward, *Rev. Mod. Phys.*, 1965, **37**, 1.
24 D. R. Kanis, M. A. Ratner and T. J. Marks, *Chem. Rev.*, 1994, **94**, 195.
25 ZINDO, 96.0/4.0.0., Molecular Simulations Inc., Cambridge, UK, 1996.
26 M. J. Frisch, G. W. Trucks, H. B. Schlegel, P. M. W. Gill, B. G. Johnson, M. A. Robb, J. R. Cheeseman, T. Keith, G. A. Petersson, J. A. Montgomery, K. Raghavachari, M. A. Al-Laham, V. G. Zakrzewski, J. V. Ortiz, J. B. Foresman, J. Cioslowski, B. B. Stefanov, A. Nanayakkara, M. Challacombe, C. Y. Peng, P. Y. Ayala, W. Chen, M. W. Wong, J. L. Andres, E. S. Replogle, R. Gomperts, R. L. Martin, D. J. Fox, J. S. Binkley, D. J. Defrees, J. Baker, J. P. Stewart, M. Head-Gordon, C. Gonzalez and J. A. Pople, Gaussian 94, Revision E.2, Gaussian, Inc., Pittsburgh, PA, 1995.
27 (*a*) J. L. Oudar and J. Chemla, *J. Chem. Phys.*, 1977, **66**, 2664; (*b*) J. L. Oudar, *J. Chem. Phys.*, 1977, **67**, 446.
28 J. March, *Advanced Organic Chemistry*, Wiley, New York, 1985, p. 23.
29 K. D. Kreuer, *Chem. Mater.*, 1996, **8**, 610.
30 S. Scheiner, *Acc. Chem. Res.*, 1994, **27**, 402.
31 X. Krokidis, V. Goncalves, A. Savin and B. Silvi, *J. Phys. Chem. A*, 1998, **102**, 5065.
32 *Solid State Protonic Conductors*, special issue of *Solid State Ionics*, 1995, **77**(1); *Solid State Protonic Conductors*, special issue of *Solid State Ionics*, 1997, **97**(1–4).
33 *Protonic Conductors*, ed. Ph. Colomban, Cambridge University Press, Cambridge, UK, 1992.
34 P. Colomban, *Ann. Chim. Sci. Mater.*, 1999, **24**, 1.
35 See for example: (*a*) P. A. Kollman and L. C. Allen, *Chem. Rev.*, 1972, **72**, 283; (*b*) W. Meyer, W. Jakubetz and P. Schuster, *Chem. Phys. Lett.*, 1973, **21**, 97.
36 C. C. Evans, M. Bagieu-Beucher, R. Masse and J.-F. Nicoud, *Chem. Mater.*, 1998, **10**, 847.